frontiers in Physics

ORIGINAL RESEARCH
published: 14 September 2020
doi: 10.3389/fphy.2020.00298

Donor-Acceptor Type Reduced Graphene-Oxide and a Tin-Selenide Nanohybrid With Broad and Ultrafast Optical Limiting Properties

Xiaoqin Li[1†], *Yingwei Wang*[1†], *Yiduo Wang*[1], *Hui Wang*[1], *Xiang Qi*[2], *Jun He*[1*] *and Si Xiao*[1*]

[1] *Hunan Key Laboratory for Super-Microstructure and Ultrafast Process, School of Physics and Electronics, Central South University, Changsha, China,* [2] *Hunan Key Laboratory for Micro-Nano Energy Materials and Devices, School of Physics and Optoelectronics, Xiangtan University, Xiangtan, China*

The non-linear absorption properties of reduced graphene-oxide (RGO) have been studied extensively but the optical limiting (OL) performance of RGO was always confined to visible light. In this study, by anchoring SnSe nanosheets onto the surface of RGO, the reduced graphene-oxide and a tin-selenide (SnSe/RGO) nanohybrid shows a broader reverse saturable absorption (RSA), ranging from 400 to 800 nm, and an enhanced non-linear optical (NLO) response. The improvement of the NLO absorption response is attributed to a multiphoton-absorption process and electron-transfer effect in this artificially constructed donor-acceptor system. Pump-probe experiments suggest a response time of ∼1.7–8 ps for the SnSe/RGO nanohybrid.

Keywords: reduced graphene-oxide (RGO), tin-selenide (SnSe), nanohybrid, donor-acceptor, optical limiting (OL)

OPEN ACCESS

Edited by:
Xiaohui Li,
Shaanxi Normal University, China

Reviewed by:
Weichun Huang,
Nantong University, China
Zhibo Liu,
Nankai University, China

***Correspondence:**
Jun He
junhe@csu.edu.cn
Si Xiao
sixiao@csu.edu.cn

[†] *These authors have contributed equally to this work*

Specialty section:
This article was submitted to Optics and Photonics, a section of the journal Frontiers in Physics

Received: *05 April 2020*
Accepted: *30 June 2020*
Published: *14 September 2020*

Citation:
Li X, Wang Y, Wang Y, Wang H, Qi X, He J and Xiao S (2020) Donor-Acceptor Type Reduced Graphene-Oxide and a Tin-Selenide Nanohybrid With Broad and Ultrafast Optical Limiting Properties. Front. Phys. 8:298. doi: 10.3389/fphy.2020.00298

INTRODUCTION

Owing to its infinitesimally small thickness and strong light-matter interaction in a broadband, graphene and its derivatives (such as graphene oxide, GO and reduced graphene oxide, RGO) has attracted tremendous attention for photonic application. In particular, many studies were done to investigate both saturable absorption (SA) [1–3] and RSA [4, 5] of two-dimensional (2D) materials, which are two typical NLO absorption properties of 2D materials. Non-linear optical properties of diverse 2D materials were investigated, including black phosphorus [6–8], transition metal dichalcogenides (TMDCs) [9, 10], topological insulator [11–13], SnS [14, 15], etc. The non-linear absorption properties of atomically-thin 2D-materials are exploited as saturable absorbers [16–19], optical diodes [20, 21], and optical limiters [22].

Once the input-beam radiation exceeds a threshold, the optical limiting (OL) material strongly attenuates the intensity of the output beam. This ensures no damage is done to human eyes and avoids potential damage to optical sensors that are exposed to high energy lasers. The range of conventional OL materials is diverse, ranging from porphyrins, phthalocyanines [23], and mixed metal-complexes [24] to carbon-based nanomaterials such as fullerenes and carbon nanotubes [25]. Recently, the OL properties of emerging 2D materials were studied in detail for MoS_2 quantum dots [26], black phosphorus [27], and TiO_2/RGO [28]. Carbon-based materials are a typically used representative 2D-system for optical limiters. Due to its unusual 2D Dirac-like band-structure, graphene exhibits zero bandgap properties. In contrast, RGO is a semiconductor with a tunable bandgap (0.5–6 eV) [29]. The non-linear absorption coefficient of RGO was determined

as 2.67 cm/GW at a wavelength of 532 nm [30]. This suggests a considerable RSA response in the visible region. To endow RGO-based OL materials with enhanced OL properties, an RGO-related nanohybrid was built using several methods. These methods include: PEG-OPE-RGO hybrids [PEG: poly(ethylene glycol), OPE: oligo (phenylene ethynylene)] [31], and SWNT/RGO hybrids (SWNTs: single-walled carbon nanotubes) [32]. Apart from the expected high OL performance, broadband OL materials are needed for many OL applications. It would be highly beneficial if such materials could be obtained by constructing an RGO-based hybrid.

2D SnSe nanosheets are an ideal candidate for the construction of RGO-based hybrids that can extend their OL properties into the near infrared region. The SnSe exhibit a narrow indirect bandgap of 0.9 eV, which results in a broad absorption-spectrum (covering the near-infrared region). Moreover, it is stable under ambient conditions with low toxicity [33]. These properties make 2D SnSe interesting for use in many optoelectronic devices, such as memory switching [34], light-emitting devices [35], and solar cells [36]. In a previous report, the RSA properties in the near infrared band were confirmed and studied [37].

In this paper, we constructed a SnSe/RGO nanohybrid using a hydrothermal method, and we confirmed a broadband OL property of an as-prepared nanohybrid, ranging from 400 to 800 nm. The dominating OL mechanism of the as-prepared hybrid was found to be a multi-photon absorption process. Moreover, using pump-probe measurements, we confirmed the optical bleaching phenomena in the as-prepared nanohybrid and revealed a response-time on the scale of picoseconds. Further, the donor-acceptor model was proposed to get insight into the underlying mechanisms of the enhanced OL performance of the nanohybrid.

RESULTS AND DISCUSSION

Characterization of SnSe/RGO Nanohybrid

The predecessors used the liquid-phase exfoliation method to produce 2D ultrathin structural materials, and proved that the crystal characteristics did not change during the stripping process [38, 39]. In this article, we added a hydrothermal intercalation process to prepare SnSe nanosheets based on the liquid-phase exfoliation method. Highly pure SnSe powder (99.5%) was purchased from Alfa Co. Inc. The 2D SnSe nanosheets were prepared via facile hydrothermal intercalation and liquid exfoliation [40, 41]. Particularly, the 0.5 g of SnSe was put into 60 ml of ethylene glycol (EG) solution containing 1 g of LiOH and kept in 50-ml of Teflon-lined autoclave at 220°C for 24 h. Then, the powder was collected by centrifugation and, following the sonication process, a few layers of SnSe nanosheets were obtained. After collecting by centrifugation and washing with water and ethanol, the desired few layers of SnSe nanosheets were obtained and dispersed in EG solution. 2D RGO was purchased from Aladdin Co. Ltd. SnSe/RGO nanocomposite was prepared using the hydrothermal method. The details can be found in our previous works [42].

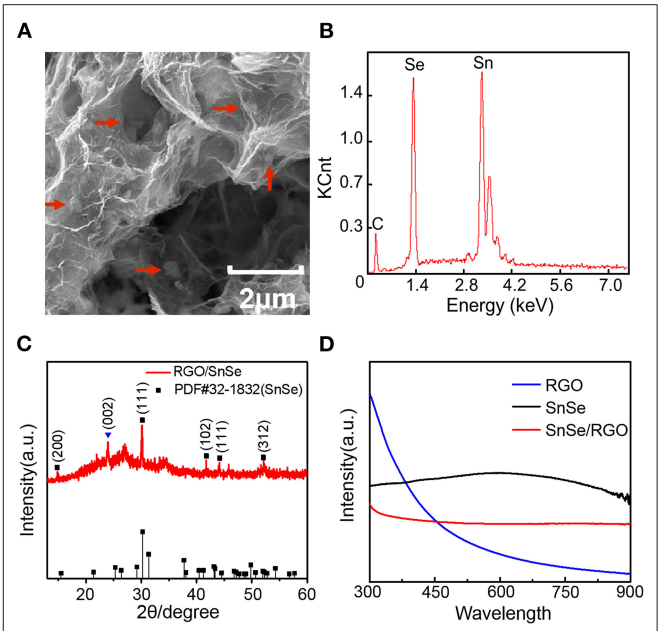

FIGURE 1 | (A) SEM image of the SnSe/RGO nanohybrid. **(B)** Energy dispersive X-ray spectroscopy of the SnSe/RGO hybrid. **(C)** XRD pattern of the SnSe/RGO nanohybrid. **(D)** UV-vis absorption spectra of the SnSe nanosheets (black line), SnSe/RGO nanohybrid (red line), and RGO nanosheets (blue line).

Figure 1A depicts a Scanning electron microscopy (SEM) (FESEM, Hitachi, Japan) image of the SnSe/RGO nano-hybrid. It can be seen that some SnSe nanosheets (red arrow) are anchored on the surface of the RGO nanosheets. **Figure 1B** shows the energy dispersive x-ray (EDX) spectroscopy result for the as-prepared SnSe/RGO nanohybrid. The EDX of the as-prepared SnSe/RGO nanohybrid displays an Se peak at 1.39 keV and Sn peaks at 3.0 keV, which are characteristic EDX peaks for Se and Sn. The phase purity and crystal structure of the as-prepared SnSe/RGO nanohybrid were identified using X-ray diffraction (Bruker D8 Advance) (see **Figure 1C**). The peak at $2\theta = 23.4^{\circ}$ is consistent with a lattice plane (002) of RGO [43]. The other diffraction peaks match the standard orthorhombic phase of SnSe well (JCPDS card no. 32–1382) [44]. **Figure 1D** shows the UV-vis absorption spectra (Cary60, Agilent) of the RGO nanosheets, the SnSe/RGO nanohybrid, and the SnSe nanosheets. Interestingly, after anchoring the SnSe nanosheets onto RGO, the SnSe/RGO hybrid shows broadband absorption covering both the visible and near infrared range. The enhancement of linear absorption increases the concentration of the photo-excited carrier, which may benefit charge transfer at the interface of the nanohybrid and induce the enhanced third-order non-linear optical response of the 2D nanohybrid.

Non-linear Optical Response

A femtosecond-pulse laser was used with a pulse width of 35 fs and pulse repetition rate of 2 kHz. Z-scan technology has higher sensitivity and stronger functionality [45]. We used the OA

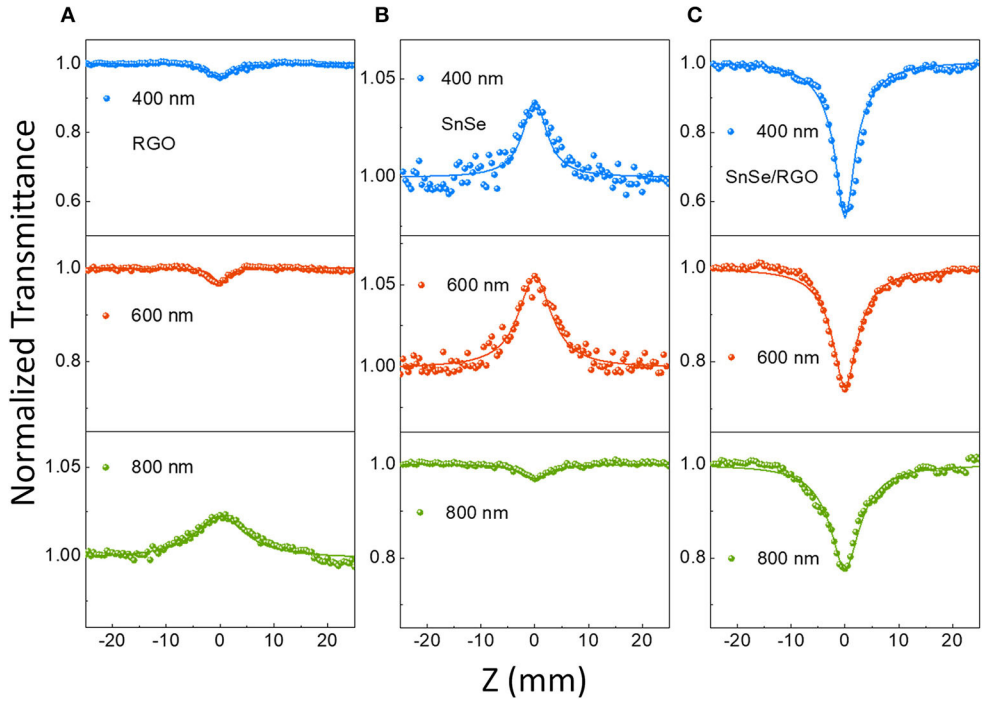

FIGURE 2 | OA Z-scan results of **(A)** RGO, **(B)** SnSe, and **(C)** SnSe/RGO with different excitation wavelengths of 400, 600, and 800 nm.

Z-scan technology to investigate the non-linear characteristics of materials. In the OA Z-scan measurement system, the incident femtosecond laser is focused by a lens, with a focal length of 150 mm. A cuvette, containing as-prepared samples, moves near the focus in the direction of the laser-light propagation (z-axis). Then, the transmitted intensity through the sample was recorded using a power meter.

Figures 2A–C shows the OA Z-scan results of SnSe, RGO, and SnSe/RGO at multiple wavelengths. The pristine SnSe shows the typical saturable absorption (SA) at 400 and 600 nm. When the excitation wavelength changes to near infrared (800 nm), the SnSe nanosheets exhibit a significant RSA response, which is similar to previous reports by Ye et al. [37]. Interestingly, for RGO, there is an RSA response with the excitation wavelength at 400 and 600 nm, which is consistent with previous studies [30]. The NLO absorption response exhibits an SA response, when the excitation wavelength is 800 nm. Such Pauli-blocking-induced optical bleaching saturable absorption has been reported previously [46]. As expected, as-prepared SnSe/RGO exhibits an RSA response that ranges from visible to the near infrared. A reasonable physical mechanism of broadened and enhanced RSA will be discussed, based on non-linear absorption parameters and the photoexcited carrier dynamic lifetime of material, in the following section.

To quantitatively analyze the OA Z-scan results, the NLO parameters of the mentioned materials were extracted by fitting the OA Z-scan curve. Based on the spatial transient Gaussian pulse model, the transmitted light intensity in the OA Z-scan experiment is [47].

$$T(z) = \frac{1}{\sqrt{\pi}q_0}\int_{-\infty}^{\infty} \ln[1 + q_0 \exp(-x^2)]dx \quad (1)$$

where, z0 is the diffraction length of the beam, $q_0 = \alpha_{NL} I_0(t) L_{eff}/(1 + z^2/z_0^2)$, $I_0(t)$ is the intensity of the light at focus, α_{NL} is the third order non-linear absorption coefficient, $L_{eff} = [1 - \exp(-\alpha_0 l)]/\alpha_0$ is known as the effective length of the sample, which is defined in terms of the linear absorption coefficient, α_0, and the effective optical path length through the sample, *l*. For the OA Z-scan results in **Figures 2A–C**, we found that the non-linear absorption coefficient of SnSe/RGO is higher than in pristine SnSe for visible light. The α_{NL} of SnSe/RGO were one order of magnitude larger than that of pristine RGO. For instance, there is an increase from 0.24 ± 0.01 cm/GW (RGO) to 2.71 ± 0.05 cm/GW (SnSe/RGO) at 400 nm. In addition, when the excitation wavelength changes to near infrared light (800 nm), the non-linear absorption coefficients were −5.30 ± 0.17 cm/GW, 11.61 ± 0.28 cm/GW, and 125.09 ± 2.73 cm/GW for pristine RGO, pristine SnSe, and SnSe/RGO, respectively. To determine the intrinsic non-linear absorption response, we extracted the imaginary part of the third-order non-linear optical susceptibility, $\mathrm{Im}\chi^{(3)}$, and the figure of merit (FOM) [48]. All extracted NLO parameters are summarized in **Table 1**.

For a better quantitative comparison, the OL parameters of this series of materials were extracted, including the OL threshold and the onset fluence. The OL threshold is defined

TABLE 1 | NLO parameters and OL parameters of RGO, SnSe, and SnSe/RGO at multi-wavelengths.

λ (nm)	Sample	I_0 (GW/cm^2)	α_{NL} (cm/GW)	Im$\chi^{(3)}$ (×10^{-13} esu)	FOM(×10^{-13} esu cm^{-1})	Onset of OL (mJ/cm^2)	OL Th.(mJ/cm^2)
400	RGO	5.45	0.24 ± 0.01	1.46 ± 0.06	0.66 ± 0.03	0.036	2.39
	SnSe	5.86	−0.19 ± 0.01	−0.56 ± 0.03	0.23 ± 0.01	/	/
	SnSe/RGO	5.43	2.71 ± 0.05	11.91 ± 0.22	4.48 ± 0.08	0.019	0.25
600	RGO	11.44	0.15 ± 0.01	1.39 ± 0.09	1.01 ± 0.07	0.015	3.88
	SnSe	7.21	−0.19 ± 0.01	−0.70 ± 0.04	0.29 ± 0.02	/	/
	SnSe/RGO	9.22	1.16 ± 0.02	7.17 ± 0.12	2.05 ± 0.04	0.025	0.60
800	RGO	0.13	−5.30 ± 0.17	−70.89 ± 2.27	54.02 ± 1.73	/	/
	SnSe	0.14	11.61 ± 0.28	55.38 ± 1.33	23.40 ± 0.56	0.004	0.055
	SnSe/RGO	0.07	125.09 ± 2.73	1067.08 ± 23.29	353.37 ± 7.71	0.0002	0.0043

as the input fluence, where the transmittance drops to 50% of the linear transmittance [49]. The onset fluence represents the laser fluence, where the OL curves start to deviate from unity [50]. **Figures 3A–C** depicts the OL properties of SnSe, RGO, and SnSe/RGO at 400, 600, and 800 nm, respectively. Compared to pristine RGO, the SnSe/RGO OL performance improved significantly. All extracted parameters are listed in **Table 1**. Taking the near infrared wavelength (800 nm) as an example, the limiting threshold of SnSe/RGO is 0.0043 mJ/cm^2, while it is 0.055 mJ/cm^2 for SnSe. The limiting threshold of SnSe/RGO is one order of magnitude below that of pristine RGO or SnSe, at the respective wavelengths. The value of the OL threshold for the SnSe/RGO is comparable with some other RSA materials, such as Sb2Se3/GO heterostructure ∼ 0.085 J/cm^2 [51], Graphene ∼ 0.10 J/cm^2 [52], MoS_2 NS ∼ 3.28 J/cm^2 [53], WS_2 NS ∼18.25 J/cm^2 [53], Au nanoparticle ∼7.5 J/cm^2 [54], etc. The lower limiting threshold indicates that nanomaterials show better optical activity and a more effective OL performance [55]. In terms of onset fluence, lower values were obtained than for pristine RGO or SnSe. Accordingly, SnSe/RGO is a potential OL candidate that may be used to shield sensor devices from high-intensity light.

To discover the dominate mechanism of such a broadened RSA performance, we performed further analyzation on the OA Z-scan results. In a conventional semiconductor system, the multi-photon absorption process usually dominates such a reverse saturable absorption. As shown in **Figure 3D**, the plot of Ln(1–T_{Norm}) vs. Ln(I) for different wavelengths confirmed multi-photon absorption induced RSA in the present system [47, 56]. The slope values for SnSe/RGO are 1.42, 1.16, and 1.18, respectively, which suggests two photon and three photon absorption takes place during the laser excitation. Additionally, the pump-probe measurements were exploited to find out the timescale of the OL response and the mechanism of significantly enhanced OL for SnSe/RGO. To exclude the effect from the solvent bubble non-linear optical scattering effect [22], all the experiments were conducted under threshold value that the solvent bubble is generated.

As shown in **Figures 4A–C**, the pump-probe results, at multiple wavelengths, for RGO, SnSe, and SnSe/RGO are shown. Using SnSe/RGO as an example, we can observe a typical negative signal near time zero in the photo-excited carrier

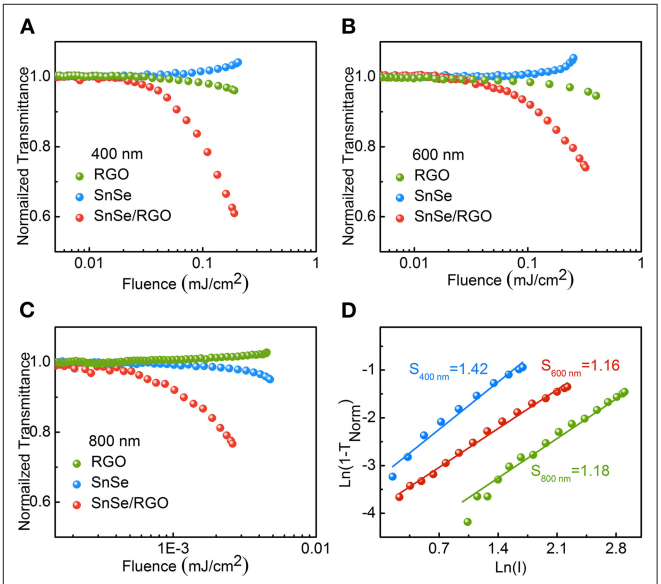

FIGURE 3 | (A–C) Normalized transmittance vs. optical energy density; **(D)** Plots of ln(1 —T_{Norm}) vs. ln(I) to determine the non-linear order of SnSe/RGO.

dynamic relaxation. The significant decrease in transmittance indicates a multi-photon-absorption-induced RSA response. Moreover, we extracted the lifetimes of the photo-excited carriers of RGO, SnSe, and SnSe/RGO at different wavelengths. For pristine RGO, the photo-excited lifetime ranges from 0.3 to 0.65 ps for different wavelengths. For pristine SnSe, on the other hand, the lifetime changed from several picoseconds (2.51 ps at 800 nm) to several tens of picoseconds (13.47 ps at 600 nm; 34.01 ps at 400 nm). As shown in **Figure 4D**, when we summarized the photoexcited carrier lifetimes, a desired median lifetime of SnSe/RGO was observed at three measurement wavelengths. This is strong evidence for electron-transfer in a donor-acceptor system. We believe that favorable energy-level alignment facilitates the above-mentioned electron transfer effect in the inset of **Figure 4D** [57, 58]. In a conventional organic polymer molecule system, the charge transfer induced enhancement third-order non-linearity of the composite was observed [59]. Moreover, these electron transfers

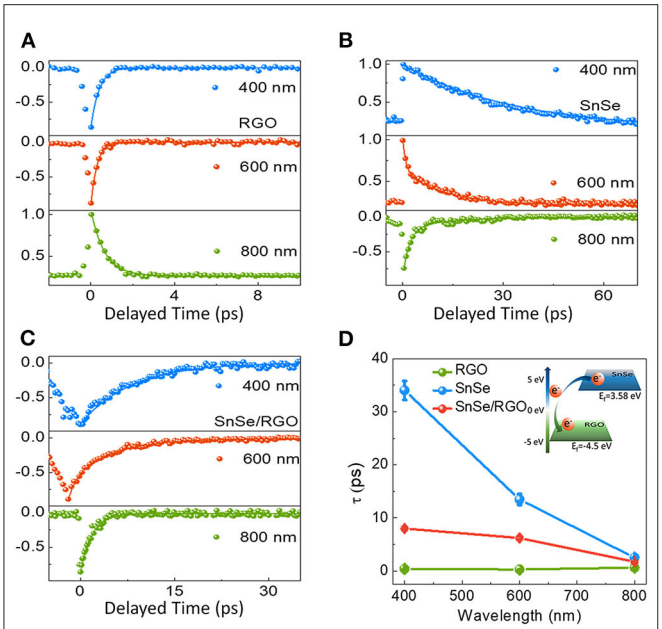

FIGURE 4 | Pump-probe experiment results of RGO **(A)**, SnSe **(B)**, and SnSe/RGO **(C)** at different excitation wavelengths: 400, 600, and 800 nm. Scatter points represent experimental data and solid lines represent fitted results. **(D)** Photo-excited carrier lifetimes at different wavelengths. In the inset of **(D)**: Schematic diagram of electron transfer. Fermi-energy level alignment of SnSe [57] and RGO [58].

increase the non-linear absorption process, which has also been clearly observed in other similar donor-acceptor 2D material systems [27].

CONCLUSION

In conclusion, the non-linear absorption and carrier dynamics of SnSe/RGO were determined using an OA Z-scan and pump-probe experiments at different wavelengths. The RSA response was obtained for the whole wavelength region, ranging from visible to near infrared. For pristine RGO this was done only for the visible range (400–600 nm). The broad RSA response of the RGO/SnSe nanohybrid can be attributed to a multi-photon absorption mechanism. The limit thresholds for the RGO/SnSe nanohybrid were 0.25 mJ/cm^2, 0.6 mJ/cm^2, and 0.055mJ/cm^2 at 400, 600, 800 nm, respectively. These are one order of magnitude below pristine RGO or SnSe, which suggests that SnSe/RGO has a stronger OL performance than pristine SnSe and RGO. The pump-probe measurements confirmed multi-photon absorption induced optical bleaching in the SnSe/RGO hybrid. The photo-excited carrier lifetime of the SnSe/RGO hybrid occurs on a picosecond timescale. We also compared the carrier lifetimes of the different samples, and the median lifetime of SnSe/RGO provides reasonable evidence for the electron transfer effect in the hybrid system, which contributes significantly to the improved OL performance of SnSe/RGO. Our results provide new opportunities to construct novel OL material systems.

DATA AVAILABILITY STATEMENT

The raw data supporting the conclusions of this article will be made available by the authors, without undue reservation.

AUTHOR CONTRIBUTIONS

SX and JH conceived the idea. XL and YinW performed the experiments. YiW and XQ conducted characterization of nanostructures. The manuscript was written through contributions of all authors. All authors have given approval to the final version of the manuscript.

FUNDING

This research was funded partially by the National Natural Science Foundation of China (Grant no. 61874141, 61875232, and 11904239), the Science and Technology Innovation Commission of Shenzhen (Grant no. JCYJ20170818141407343), and Fundamental Research Funds for the Central Universities of Central South University (2019zzts415).

REFERENCES

1. Liu X, Guo Q, Qiu J. Emerging low-dimensional materials for nonlinear optics and ultrafast photonics. *Adv Mater.* (2017) **29**:1605886. doi: 10.1002/adma.201605886
2. Yu S, Wu X, Wang Y, Guo X, Tong L. 2D materials for optical modulation: challenges and opportunities. *Adv Mater.* (2017) **29**:1606128. doi: 10.1002/adma.201606128
3. Guo B, Xiao QL, Wang SH, Zhang H. 2D layered materials: synthesis, nonlinear optical properties, device applications. *Laser Photonics Rev.* (2019) **13**:1800327. doi: 10.1002/lpor.201800327
4. Dini D, Calvete MJ, Hanack M. Nonlinear optical materials for the smart filtering of optical radiation. *Chem Rev.* (2016) **116**:13043–233. doi: 10.1021/acs.chemrev.6b00033
5. Liaros N, Fourkas JT. The characterization of absorptive nonlinearities. *Laser Photonics Rev.* (2017) **11**:1700106. doi: 10.1002/lpor.201700106
6. Chen Y, Jiang G, Chen S, Guo Z, Yu X, Zhao C, et al. Mechanically exfoliated black phosphorus as a new saturable absorber for both Q-switching and Mode-locking laser operation. *Opt. Express.* (2015) **23**:12823–33. doi: 10.1364/OE.23.012823
7. Wang Y, Huang G, Mu H, Lin S, Chen J, Xiao S, et al. Ultrafast recovery time and broadband saturable absorption properties of black phosphorus suspension, *Appl Phys Lett.* (2015) **107**:091905. doi: 10.1063/1.4930077
8. Wang YW, Liu S, Zeng BW, Huang H, Xiao J, Li JB, et al. Ultraviolet saturable absorption and ultrafast carrier dynamics in ultrasmall black phosphorus quantum dots. *Nanoscale.* (2017) **9**:4683–90. doi: 10.1039/C6NR09235G
9. Li Z, Li R, Pang C, Zhang Y, Yu H, Chen F. WSe_2 as a saturable absorber for multi-gigahertz Q-switched mode-locked waveguide lasers [Invited]. *Chin Opt Lett.* (2019) **17**:020013. doi: 10.3788/COL201917.020013
10. Huang J, Dong N, McEvoy N, Wang L, Coileain CO, Wang H, et al. Surface-state assisted carrier recombination and optical nonlinearities in bulk to 2D nonlayered PtS. *ACS Nano.* (2019) **13**:13390–402. doi: 10.1021/acsnano.9b06782

11. Shi B, Miao L, Wang Q, Du J, Tang P, Liu J, et al. Broadband ultrafast spatial self-phase modulation for topological insulator Bi2Te$_3$ dispersions, *Appl Phys Lett.* (2015) **107**:151101. doi: 10.1063/1.4932590
12. Wang Y, Mu H, Li X, Yuan J, Chen J, Xiao S, et al. Observation of large nonlinear responses in a graphene-Bi2Te3 heterostructure at a telecommunication wavelength, *Appl Phys Lett.* (2016) 1**08**:221901. doi: 10.1063/1.4953072
13. Wang Y, Liu S, Yuan J, Wang P, Chen J, Li J, et al. Ultra-broadband nonlinear saturable absorption for two-dimensional Bi_2TexSe_3-x nanosheets, *Sci Rep.* (2016) **6**:33070. doi: 10.1038/srep33070
14. Xie Z, Zhang F, Liang Z, Fan T, Li Z, Jiang X, et al. Revealing of the ultrafast third-order nonlinear optical response and enabled photonic application in two-dimensional tin sulfide, *Photonics Res.* (2019) **7**:494–502. doi: 10.1364/PRJ.7.000494
15. Wu L, Xie Z, Lu L, Zhao J, Wang Y, Jiang X, et al. Few-layer tin sulfide: a promising black-phosphorusanalogue 2D material with exceptionally large nonlinear optical response, high stability, and applications in all-optical switching and wavelength conversion. *Adv Opt Mater.* (2018) **6**:1700985. doi: 10.1002/adom.201700985
16. Wang Y, Chen K, Hao H, Yu G, Zeng B, Wang H, et al. Engineering ultrafast charge transfer in a bismuthene/perovskite nanohybrid. *Nanoscale.* (2019) **11**:2637–43. doi: 10.1039/C9NR00058E
17. Zou X, Leng Y, Li Y, Feng Y, Zhang P, Hang Y, et al. Passively Q-switched mode-locked Tm:LLF laser with a MoS_2 saturable absorber. *Chin Opt Lett.* (2015) **13**:081405. doi: 10.3788/COL201513.081405
18. Chen K, Wang Y, Liu J, Kang J, Ge Y, Huang W, et al. *In situ.* preparation of a $CsPbBr_3$/black phosphorus heterostructure with an optimized interface and photodetector application, *Nanoscale.* (2019) **11**:16852–9. doi: 10.1039/C9NR06488E
19. You JW, Bongu SR, Bao Q, Panoiu NC. Nonlinear optical properties and applications of 2D materials: theoretical and experimental aspects. *Nanophotonics.* (2018) **8**:63. doi: 10.1515/nanoph-2018-0106
20. Wu L, Dong Y, Zhao J, Ma D, Huang W, Zhang Y, et al. Kerr Nonlinearity in 2D graphdiyne for passive photonic diodes. *Adv Mater.* (2019) **31**:1807981. doi: 10.1002/adma.201807981
21. Dong Y, Chertopalov S, Maleski K, Anasori B, Hu L, Bhattacharya S, et al. Saturable absorption in 2D Ti_3C_2 MXene thin films for passive photonic diodes. *Adv Mater.* (2018) **30**:1705714. doi: 10.1002/adma.201705714
22. Chen Y, Bai T, Dong N, Fan F, Zhang S, Zhuang X, et al. Graphene and its derivatives for laser protection. *Prog Mater Sci.* (2016) **84**:118–57. doi: 10.1016/j.pmatsci.2016.09.003
23. Chen Y, Hanack M, Araki Y, Ito O. Axially modified gallium phthalocyanines and naphthalocyanines for optical limiting. *Chem Soc Rev.* (2005) **34**:517–29. doi: 10.1039/b416368k
24. Zhou GJ, Wong WY. Organometallic acetylides of Pt(II), Au(I) and Hg(II) as new generation optical power limiting materials. *Chem Soc Rev.* (2011) **40**:2541–66. doi: 10.1039/c0cs00094a
25. Wang J, Chen Y, Blau WJ. Carbon nanotubes and nanotube composites for nonlinear optical devices. *J Mater Chem.* (2009) **19**:7425–43. doi: 10.1039/b906294g
26. Jiang P, Zhang B, Liu Z, Chen Y. MoS_2 quantum dots chemically modified with porphyrin for solid-state broadband optical limiters. *Nanoscale.* (2019) **11**:20449–55. doi: 10.1039/C9NR06604G
27. Wang K, Dong N, Liu Z, Shi M, Zhang B, Wang J, et al. Donor-acceptor type black phosphorus nanosheets covalently functionalized with a conjugated polymer for laser protection. *Polym Chem.* (2019) **10**:6003–9. doi: 10.1039/C9PY01284B
28. Ren Y, Zhao L, Zou Y, Song L, Dong N, Wang J. Effects of different TiO_2 particle sizes on the microstructure and optical limiting properties of TiO_2/reduced graphene oxide nanocomposites. *Nanomaterials.* (2019) **9**:730. doi: 10.3390/nano9050730
29. Eda G, Lin YY, Mattevi C, Yamaguchi H, Chen HA, Chen IS, et al. Blue photoluminescence from chemically derived graphene oxide. *Adv Mater.* (2010) **22**:505–9. doi: 10.1002/adma.200901996
30. Shi HF, Wang C, Sun ZP, Zhou YL, Jin KJ, Redfern SAT, et al. Tuning the nonlinear optical absorption of reduced graphene oxide by chemical reduction. *Opt Express.* (2014) **22**:19375–82. doi: 10.1364/OE.22.019375
31. He TC, Qi XY, Chen R, Wei J, Zhang H, Sun HD. Enhanced optical nonlinearity in noncovalently functionalized amphiphilic graphene composites. *Chempluschem.* (2012) **77**:688–93. doi: 10.1002/cplu.201200113
32. Dong XC, Xing GC, Chan-Park MB, Shi WH, Xiao N, Wang J, et al. The formation of a carbon nanotube-graphene oxide core-shell structure and its possible applications. *Carbon.* (2011) **49**:5071–8. doi: 10.1016/j.carbon.2011.07.025
33. Shi G, Kioupakis E. Anisotropic spin transport and strong visible-light absorbance in few-layer SnSe and GeSe. *Nano Lett.* (2015) **15**:6926–31. doi: 10.1021/acs.nanolett.5b02861
34. Chung KM, Wamwangi D, Woda M, Wuttig M, Bensch W. Investigation of SnSe, $SnSe_2$, and Sn_2Se_3 alloys for phase change memory applications. *J Appl Phys.* (2008) **103**:083523. doi: 10.1063/1.2894903
35. Baumgardner WJ, Choi JJ, Lim YF, Hanrath T. SnSe nanocrystals: synthesis, structure, optical properties, surface chemistry. *J Am Chem Soc.* (2010) **132**:9519–21. doi: 10.1021/ja1013745
36. Liu S, Guo X, Li M, Zhang WH, Liu X, Li C. Solution-phase synthesis and characterization of single-crystalline SnSe nanowires. *Angew Chem Int Edit.* (2011) **50**:12050–3. doi: 10.1002/anie.201105614
37. Ye Y, Xian Y, Cai J, Lu K, Liu Z, Shi T, et al. Linear and nonlinear optical properties of few-layer exfoliated SnSe nanosheets. *Adv Opt Mater.* (2019) **7**:1800579. doi: 10.1002/adom.201800579
38. Xing C, Xie Z, Liang Z, Liang W, Fan T, Ponraj JS, et al. 2D nonlayered selenium nanosheets: facile synthesis, photoluminescence, ultrafast photonics. *Adv Optical Mater.* (2017) **5**:1700884. doi: 10.1002/adom.201700884
39. Xie Z, Xing C, Huang W, Fan T, Li Z, Zhao J, et al. Ultrathin 2D nonlayered tellurium nanosheets: facile liquid-phase exfoliation, characterization, and photoresponse with high performance and enhanced stability. *Adv Funct Mater.* (2018) **28**:1705833. doi: 10.1002/adfm.201705833
40. Ren L, Qi X, Liu YD, Hao GL, Huang ZY, Zou XH, et al. Large-scale production of ultrathin topological insulator bismuth telluride nanosheets by a hydrothermal intercalation and exfoliation route. *J Mater Chem.* (2012) **22**:4921–6. doi: 10.1039/c2jm15973b
41. Chujun Zhao, Zhang H, Qi X, Chen Y, Wang Z, Wen S, et al. Ultra-short pulse generation by a topological insulator based saturable absorber. *Appl Phys Lett.* (2012) **101**:211106. doi: 10.1063/1.4767919
42. Qiao H, Huang ZY, Ren XH, Yao H, Luo SW, Tang PH, et al. Photoresponse improvement in liquid-exfoliated SnSe nanosheets by reduced graphene oxide hybridization. *J Mater Sci.* (2018) **53**:4371–7. doi: 10.1007/s10853-017-1878-8
43. Fan ZJ, Wang K, Wei T, Yan J, Song LP, Shao B. An environmentally friendly and efficient route for the reduction of graphene oxide by aluminum powder. *Carbon.* (2010) **48**:1686–9. doi: 10.1016/j.carbon.2009.12.063
44. Ren X, Qi X, Shen Y, Xu G, Li J, Li Z, et al. Synthesis of SnSe nanosheets by hydrothermal intercalation and exfoliation route and their photoresponse properties. *Mater Sci Eng.* (2016) **214**:46–50. doi: 10.1016/j.mseb.2016.09.001
45. Sheik-Bahae M, Said AA, Van Stryland EW. High-sensitivity, single-beam n_2 measurements, *Opt Lett.* (1989) **14**:955–7. doi: 10.1364/OL.14.000955
46. Zhao X, Liu Z, Yan W, Wu Y, Zhang X, Chen Y, et al. Ultrafast carrier dynamics and saturable absorption of solutionprocessable few-layered graphene oxide. *Appl Phys Lett.* (2011) **98**:121905. doi: 10.1063/1.3570640
47. He J, Qu Y, Li H, Mi J, Ji W. Three-photon absorption in ZnO and ZnS crystals. *Opt Express.* (2005) **13**:9235–47. doi: 10.1364/OPEX.13.009235
48. Wang K, Wang J, Fan J, Lotya M, O'Neill A, Fox D, et al. Ultrafast saturable absorption of two-dimensional MoS_2 nanosheets. *ACS Nano.* (2013) **7**:9260–7. doi: 10.1021/nn403886t
49. Ekbote A, Patil PS, Maidur SR, Chia TS, Quah CK. Structural, third-order optical nonlinearities and figures of merit of (E)-1-(3-substituted phenyl)-3-(4-fluorophenyl) prop-2-en-1-one under CW regime: new chalcone derivatives for optical limiting applications. *Dyes Pigments.* (2017) **139**:720–9. doi: 10.1016/j.dyepig.2017.01.002
50. Feng M, Sun RQ, Zhan HB, Chen Y. Decoration of carbon nanotubes with CdS nanoparticles by polythiophene interlinking for optical limiting enhancement. *Carbon.* (2010) **48**:1177–85. doi: 10.1016/j.carbon.2009.11.041
51. Yadav RK, Aneesh1 RSJ, Salvi1 JJM, Jain H, Adarsh KV. Giant enhancement of nonlinear absorption in graphene oxide—Sb_2Se_3 nanowire heterostructure. *J Appl Phys.* (2019) 125:025702. doi: 10.1063/1.5053721

52. Lim GK, Chen ZL, Clark J, Goh RGS, Ng WH, Tan HW, et al. Giant broadband nonlinear optical absorption response in dispersed graphene single sheets. *Nat Photonics.* (2011) **5**:554–60. doi: 10.1038/nphoton.2011.177
53. Dong N, Li Y, Feng Y, Zhang S, Zhang X, Chang C, et al. Optical limiting and theoretical modelling of layered transition metal dichalcogenide nanosheets. *Sci Rep.* (2015) **5**:14646. doi: 10.1038/srep14646
54. Polavarapu L, Venkatram N, Ji W, Xu QH. Optical-limiting properties of oleylamine-capped gold nanoparticles for both femtosecond and nanosecond laser pulses. *ACS Appl Mater Interfaces.* (2009) **1**:2298–303. doi: 10.1021/am900442u
55. Shkir M, Arif M, Ganesh V, Manthrammel MA, Singh A, Yahia IS, et al. Investigation on structural, linear, nonlinear and optical limiting properties of sol-gel derived nanocrystalline Mg doped ZnO thin films for optoelectronic applications. *J Mol Struct.* (2018) **1173**:375–84. doi: 10.1016/j.molstruc.2018.06.105
56. He J, Ji W, Mi J, Zheng Y, Ying JY. Three-photon absorption in water-soluble ZnS nanocrystals. *Appl Phys Lett.* (2006) **88**:181114. doi: 10.1063/1.2198823
57. Peng K, Lu X, Zhan H, Hu S, Tang X, Wang G, et al. Broad temperature plateau for high ZTs in heavily doped p-type SnSe single crystals. *Energ Environ Sci.* (2016) **9**:454–60. doi: 10.1039/C5EE03366G
58. Mondal S, Sudhu S, Bhattacharya S, Saha SK. Strain-induced tunable band gap and morphology-dependent photocurrent in RGO-CdS nanostructures. *J Mater Chem.* (2015) **119**:27749–58. doi: 10.1021/acs.jpcc.5b08116
59. Lutherdavies B. Third-order nonlinear optical organic materials for photonic switching. *Curr Opin Solid State Mater Sci.* (1997) **2**:213–9. doi: 10.1016/S1359-0286(97)80068-X

Conflict of Interest: The authors declare that the research was conducted in the absence of any commercial or financial relationships that could be construed as a potential conflict of interest.